

## Ground motion scaling methods for linear-elastic structures: an integrated experimental and analytical investigation

A. P. O'Donnell<sup>1</sup>, Y. C. Kurama<sup>1,\*</sup>,†, E. Kalkan<sup>2</sup>, A. A. Taflanidis<sup>1</sup> and O. A. Beltsar<sup>1</sup>

<sup>1</sup>*Civil and Environmental Engineering and Earth Sciences, Univ. of Notre Dame, Notre Dame, IN 46556, U.S.A.*

<sup>2</sup>*Earthquake Science Center, United States Geological Survey, Menlo Park, CA 94025, U.S.A.*

### SUMMARY

The task of selecting and scaling an appropriate set of ground motion records is one of the most important challenges facing practitioners in conducting dynamic response history analyses for seismic design and risk assessment. This paper describes an integrated experimental and analytical evaluation of selected ground motion scaling methods for linear-elastic building frame structures. The experimental study is based on the shake table testing of small-scale frame models with four different fundamental periods under ground motion sets that have been scaled using different methods. The test results are then analytically extended to a wider range of structural properties to assess the effectiveness of the scaling methods in reducing the dispersion and increasing the accuracy in the seismic displacement demands of linear-elastic structures, also considering biased selection of ground motion subsets. For scaling methods that are based on a design estimate of the fundamental period of the structure, effects of possible errors in the estimated period are investigated. The results show that a significant reduction in the effectiveness of these scaling methods can occur if the fundamental period is not estimated with reasonable certainty. Copyright © 2012 John Wiley & Sons, Ltd.

Received 12 October 2011; Revised 26 September 2012; Accepted 1 October 2012

**KEY WORDS:** dynamic response history analysis; ground motion selection and scaling; linear-elastic structures; seismic design

### 1. INTRODUCTION

This paper describes an integrated experimental and analytical investigation on the scaling of ground motion records for use in the dynamic response history analysis (RHA) of linear-elastic structures. In recent years, as performance-based seismic design considerations have become pre-requisite for controlling the level of structural and non-structural damage during an earthquake, the use of RHA has gained utmost importance. This rigorous analysis method requires, as input, a suite of ground motion records that have been selected and modified (i.e., scaled) appropriately to make them compatible with the site-specific hazard level(s) considered (e.g., service basis earthquake; design basis earthquake). Ground motion scaling has a large impact on RHA results, governing the outcome and amount of uncertainty for seismic design. Ironically, this is also the single task with the least guidance provided in current building codes and provisions, resulting in the use of mostly subjective choices in design.

Although the seismic design of most civil engineering structures is based on significant nonlinear behavior, the dynamic response of linear-elastic systems is relevant for many applications such as critical structures that are required to remain essentially linear elastic, very tall or very short structures, and structures under low-intensity ground motions, where significant nonlinearity is not

\*Correspondence to: Yahya C. Kurama, Civil and Environmental Engineering and Earth Sciences, Univ. of Notre Dame, 156 Fitzpatrick Hall, Notre Dame, IN 46556, U.S.A.

†E-mail: ykurama@nd.edu

expected (e.g., service level response). Considering these applications, this paper presents the measured response from small-scale shake table experiments of linear-elastic multi-story building frame structures under ground motion sets that have been scaled using different methods. The test results are then extended to a wider range of structural properties using a calibrated analytical model to assess the effectiveness of the scaling methods in reducing the dispersion and increasing the accuracy in the lateral displacement demands.

The previous research on ground motion scaling [e.g., 1–21] has been based solely on numerical simulations with no experimental data available for the validation of the results. Furthermore, for scaling methods that depend on an estimated fundamental period for the structure, no consideration has been given on the impact of errors in the estimated period. Although previous shake table experiments of small-scale linear-elastic structures are available in the literature [e.g., 22–25], none of these studies has investigated ground motion scaling. These factors have contributed to a lack of consensus regarding the scaling methods that are best suited to achieve reliable, robust median seismic demand estimates over a range of structural properties. The shake table tests described in this paper form the first experimental study to evaluate the accuracy (that is, ability to provide accurate estimates of the median demands as if a much larger set of records were used) and efficiency (that is, ability to minimize the number of records needed to reliably obtain these accurate median demand estimates) of ground motion scaling methods, also considering biased selection of ground motion subsets and including the effects of inaccuracies in the estimated building period.

## 2. CURRENT PRACTICE AND CHALLENGES

Procedures for selecting and scaling ground motion records for a site-specific seismic hazard analysis are broadly described in current building codes. The ground motion selection and scaling procedures in the International Building Code [26] and California Building Code [27] are based on ASCE 7–05 [28]. According to the ASCE provisions, the average 5%-damped linear-elastic acceleration response spectrum for a set of scaled records should not be less than the design spectrum over the period range from  $0.2 T_1$  to  $1.5 T_1$ , where  $T_1$  is the fundamental vibration period of the structure being designed. The provisions do not provide any specific ground motion scaling guidelines to achieve this requirement on the average spectrum. The design value of an engineering demand parameter (EDP)—member deformations, lateral displacements, floor accelerations, and others—is taken as the average value of the EDP if seven or more records are used in the analysis, or its maximum value over all ground motions if the structure is analyzed for less than seven records (ASCE 7–05 requires a minimum of three records). These requirements are the same as those in ASCE 7–10 [29]. The required number of records prescribed by ASCE-7 is based on engineering judgment instead of a comprehensive evaluation [30].

Scaling methods that result in inaccurate estimates of the median EDPs, with significant dispersion in the demands from the individual records in an ensemble, can drastically alter the design outcome depending on the records selected, thus diminishing engineering confidence. To demonstrate the challenges for current practice, Figure 1 shows the measured peak roof drift demands,  $\Delta_r$  [i.e., peak roof relative (with respect to the base) lateral displacement,  $D_r$ , divided by the height to the roof] for one of the test structures described in this paper (Frame LE2) subjected to a suite of 25 ground motion records satisfying the ASCE 7–10 [29] scaling requirement. The ground motion intensity is plotted on the  $x$ -axis using the spectral acceleration of each ground motion at the fundamental period of the structure,  $S_a(T_1)$ . It can be seen that the drift demands from the ground motion suite range from a minimum of slightly less than 0.1% to a maximum of about 1.2%. It is clear that if only the peak demand from three records were used in design, as allowed by ASCE 7–10, then the design outcome (i.e., over-design, under-design, or satisfactory) can be drastically altered depending on the records selected. Although the use of a larger number of records may improve the median EDP estimates, this approach may not be practical. Further, the use of a large number of records does not answer the question on how these records should be scaled for a given design scenario [30].

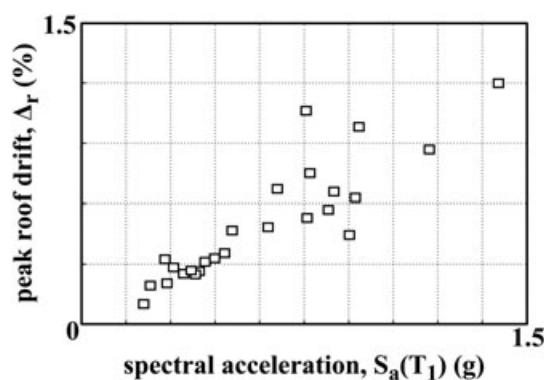


Figure 1. Peak  $\Delta_r$  demands for Frame LE2.

### 3. BACKGROUND

Previous research on ground motion scaling has primarily focused on ‘intensity-based’ methods over ‘spectral matching.’ Spectral matching modifies the frequency content or phasing of the record to match its response spectrum to a target spectrum, whereas intensity-based methods preserve the non-stationary content of the ground motion record and only modify its amplitude using one or more intensity measures (IMs) to determine the scaling factors. The earliest approach to the problem is the scaling of ground motions to match a target peak ground acceleration, *PGA*, which has been shown to produce inaccurate median EDP estimates with large dispersion [2–4, 12]. Other scalar IMs, such as the effective peak acceleration, Arias intensity, and effective peak velocity, have also been found inaccurate and inefficient [15]. On the other hand, the maximum incremental velocity (*MIV*, defined as the maximum area under the acceleration time-history of a ground motion between two consecutive zero acceleration crossings), which captures the impulsive characteristics of the record, can be a good indicator of the seismic demands [15, 31–33].

None of the mentioned IMs consider any property of the structure being designed in determining the ground motion scaling factors. Including a vibration property of the structure can lead to improved methods. For example, scaling records to a target linear-elastic spectral acceleration,  $S_a(T_1)$  at the fundamental period of the structure,  $T_1$ , can provide improved EDP estimates for structures whose response is dominated by their first mode of vibration [13]. However, it has been shown that this scaling method becomes less accurate and less efficient for taller structures with significant higher mode response or for structures responding far into the nonlinear range [15, 16]. To consider higher mode response, a scalar IM that combines the spectral accelerations  $S_a(T_1)$  and  $S_a(T_2)$  at the first two periods, as well as a vector IM based on  $S_a(T_1)$  and the  $S_a(T_1)/S_a(T_2)$  ratio have been studied [6]. Although this vector IM improves accuracy, it remains inefficient for near-fault records with a dominant velocity pulse.

### 4. GROUND MOTION RECORDS AND SCALING METHODS

Because of a lack of specific guidelines, practitioners often select ground motion records on the basis solely of distance, site conditions, and magnitude of the characteristic event expected to dominate the seismic hazard. For the selection of the ground motions in this study, a set of criteria and identification algorithms [34] were adopted to distinguish earthquake records on the basis of their characteristic attributes associated with source, directivity, site, and/or basin effects (e.g., cyclic versus impulsive records; records with high, mid, or low frequency content; short or long duration records). Basin, duration, and pulse attributes of the records were investigated by frequency domain analyses; whereas, directivity and fling attributes [35, 36] were identified from the orientation of the accelerometers relative to the fault strike. These attributes were then used to categorize a large library of records [37] to facilitate the selection of the most suitable ground motions for different site-specific hazard

conditions. On the basis of this refinement and pre-selection process, a suite of 39 near-fault strong ground motions, recorded within 20 km of the causative fault in shallow-crustal tectonic environments, were compiled as shown in Table I. It should be noted that although all 39 records were used in the analytical investigation, the analytical results indicated that 14 of the records would result in significant nonlinearity of the beam-column connections in the physical laboratory test structure. Therefore, these 14 records were excluded from the experimental investigation, resulting in the 25 records indicated by the gray shaded rows of Table I for use in shake table testing.

Table I. Selected near-fault ground motion records.

Record ID	Earthquake Name	Station Name	Year	Magnitude $M_w$	Fault Dist. (km)	$V_{530}$ (m/s)	$PGA$ (g)	$MIV$ (m/s)
1058-E	Duzce, Turkey	Lamont 1058	1999	7.1	0.2	425	0.111	0.256
1059-N	Duzce, Turkey	Lamont 1059	1999	7.1	4.2	425	0.147	0.103
1061-E	Duzce, Turkey	Lamont 1061	1999	7.1	11.5	481	0.134	0.144
1062-E	Duzce, Turkey	Lamont 1062	1999	7.1	9.2	338	0.257	0.256
375-N	Duzce, Turkey	Lamont 375	1999	7.1	3.9	425	0.970	0.612
531-N	Duzce, Turkey	Lamont 531	1999	7.1	8.0	660	0.159	0.160
BOL090	Duzce, Turkey	Bolu	1999	7.1	12.0	326	0.822	1.237
DZC270	Duzce, Turkey	Duzce	1999	7.1	6.7	276	0.535	1.108
A-CTR270	Irpinia, Italy	Calitri	1980	6.9	17.6	600	0.176	0.348
AMA090	Kobe, Japan	Amagasaki	1995	6.9	11.3	256	0.363	0.825
FKS090	Kobe, Japan	Fukushima	1995	6.9	17.9	256	0.216	0.543
KJM000	Kobe, Japan	KJMA	1995	6.9	1.0	312	0.821	1.586
NIS090	Kobe, Japan	Nishi-Akashi	1995	6.9	7.1	609	0.503	0.588
PRI000	Kobe, Japan	Port Island (0 m)	1995	6.9	3.3	198	0.315	1.494
SHI000	Kobe, Japan	Shin-Osaka	1995	6.9	19.1	256	0.243	0.501
TAK090	Kobe, Japan	Takatori	1995	6.9	1.5	256	0.616	1.862
TAZ090	Kobe, Japan	Takarazuka	1995	6.9	0.3	312	0.694	1.050
BRN090	Loma Prieta, CA	BRAN	1989	6.9	10.7	376	0.501	0.710
CAP000	Loma Prieta, CA	Capitola	1989	6.9	15.2	289	0.529	0.625
CLS000	Loma Prieta, CA	Corralitos	1989	6.9	3.9	463	0.644	0.829
G02000	Loma Prieta, CA	Gilroy Array #2	1989	6.9	11.1	271	0.367	0.507
G03000	Loma Prieta, CA	Gilroy Array #3	1989	6.9	12.8	350	0.555	0.537
G04000	Loma Prieta, CA	Gilroy Array #4	1989	6.9	14.3	222	0.417	0.547
G06090	Loma Prieta, CA	Gilroy Array #6	1989	6.9	18.3	664	0.170	0.208
GIL067	Loma Prieta, CA	Gilroy-Gavilan Coll.	1989	6.9	10.0	730	0.357	0.331
GOF160	Loma Prieta, CA	Gilroy-Historic Bldg.	1989	6.9	11.0	339	0.284	0.777
LGP090	Loma Prieta, CA	LGPC	1989	6.9	5.0	1070	0.605	0.615
LOB000	Loma Prieta, CA	UCSC Lick Observatory	1989	6.9	18.4	714	0.450	0.290
SJTE225	Loma Prieta, CA	San Jose-Santa Teresa Hills	1989	6.9	14.7	672	0.275	0.239
STG000	Loma Prieta, CA	Saratoga-Aloha Ave	1989	6.9	8.5	371	0.512	0.588
UC2090	Loma Prieta, CA	UCSC	1989	6.9	18.5	714	0.396	0.200
WAH090	Loma Prieta, CA	WAHO	1989	6.9	17.5	376	0.638	0.466
WVC270	Loma Prieta, CA	Saratoga-W Valley Coll.	1989	6.9	9.3	371	0.332	0.673
CPM000	Cape Mendocino, CA	Cape Mendocino	1992	7.0	7.0	514	1.497	1.196
FOR000	Cape Mendocino, CA	Fortuna-Fortuna Blvd	1992	7.0	19.9	457	0.116	0.372
PET090	Cape Mendocino, CA	Petrolia	1992	7.0	8.2	713	0.662	1.232
RIO360	Cape Mendocino, CA	Rio Dell Overpass-FF	1992	7.0	14.3	312	0.549	0.737
HEC090	Hector Mine, CA	Hector	1999	7.1	12.0	685	0.337	0.480
I-ELC180	Imperial Valley-02	El Centro Array #9	1940	6.9	6.1	213	0.313	0.462

Note: Only the records in the shaded rows were used in the shake table testing program.

The following six suites of ground motions were utilized in this research:

- GM[Uns] - Unscaled ground motions from Table I;
- GM[ASCE7] - Ground motions in Table I scaled on the basis of ASCE 7–10 [29];
- GM[MIV] - Ground motions in Table I scaled to the median  $MIV$  of the suite;
- GM[ $S_a(T_1)$ ] - Ground motions in Table I scaled to the median linear-elastic single-DOF spectral acceleration at the fundamental period of the structure,  $T_1$ ;

- GM[ $S_a(1.3 T_1)$ ] - Ground motions in Table I scaled to the median linear-elastic spectral acceleration at  $1.3 T_1$ ;
- GM[ $S_a(0.7 T_1)$ ] - Ground motions in Table I scaled to the median linear-elastic spectral acceleration at  $0.7 T_1$ .

For demonstration purposes, Figure 2 shows the linear-elastic acceleration response spectra of the ground motion records in each suite used in the study of Frame LE2. The median (geometric mean) response spectrum of the unscaled records in Table I was used as the target response spectrum for scaling methods that require a target spectrum as part of their definition [i.e., ASCE7,  $S_a(T_1)$ ,  $S_a(1.3 T_1)$ , and  $S_a(0.7 T_1)$  methods]. In addition to the intensity-based scaling of the ground motions, each record was also modified with a length-scale of  $S_L = 1/10$  and a time-scale of  $S_T = 1/3$  on the basis of the similitude requirements of the small-scale model test structure. The ground motion spectra in Figure 2 are plotted for the measured viscous damping,  $\xi$  for Frame LE2, with the different damping factors in the different plots representing the measured displacement-dependent damping properties of the structure as described later. Note that this is a different approach from previous studies where 5% damping has been typically used to match the target design spectra from building codes. Because the current study is based on a set of physical structures, the measured properties of these structures were used as much as possible to determine the true accuracy and effectiveness of each scaling method (i.e., when no design approximations are made). To evaluate the potential impact of this decision, a Student's  $t$ -test analysis [38] was conducted to investigate the effect of the damping ratio on the ground motion scaling factors, showing that varying the damping ratio between the measured value and the design value of 5% does not have a statistically significant effect on the scaling factors at the generally accepted 0.05 (5%) significance level.

The vertical dashed lines in Figure 2 depict the measured fundamental period,  $T_1$  for Frame LE2. Errors in period estimation (in other words, design approximations to the actual period) could significantly affect the results from the  $S_a(T_1)$  method because of the dependence of the method on a single period. To investigate the effects of uncertainties in structural period estimation (i.e., inaccuracies in period estimation that could be expected in typical design practice), suites GM[ $S_a(1.3 T_1)$ ] and GM[ $S_a(0.7 T_1)$ ] were used to introduce a 30% error in  $T_1$  (i.e., instead of  $T_1$ , a period of  $0.7 T_1$  or  $1.3 T_1$  was used to determine the target  $S_a$  value from the median spectrum). This error range was determined on the basis of the paper by Goel and Chopra [39], which shows a wide range for the measured periods of steel moment resisting frames from about  $0.70 T_L$  to about  $1.3 T_U$ , where  $T_L$  is the approximate period equation in ASCE 7–10 and  $T_U$  represents the upper limit period equation. It should be emphasized that the actual error in the estimated period of a building can be different than the values used in this study; and thus, the results obtained from the GM[ $S_a(1.3 T_1)$ ] and GM[ $S_a(0.7 T_1)$ ] suites should

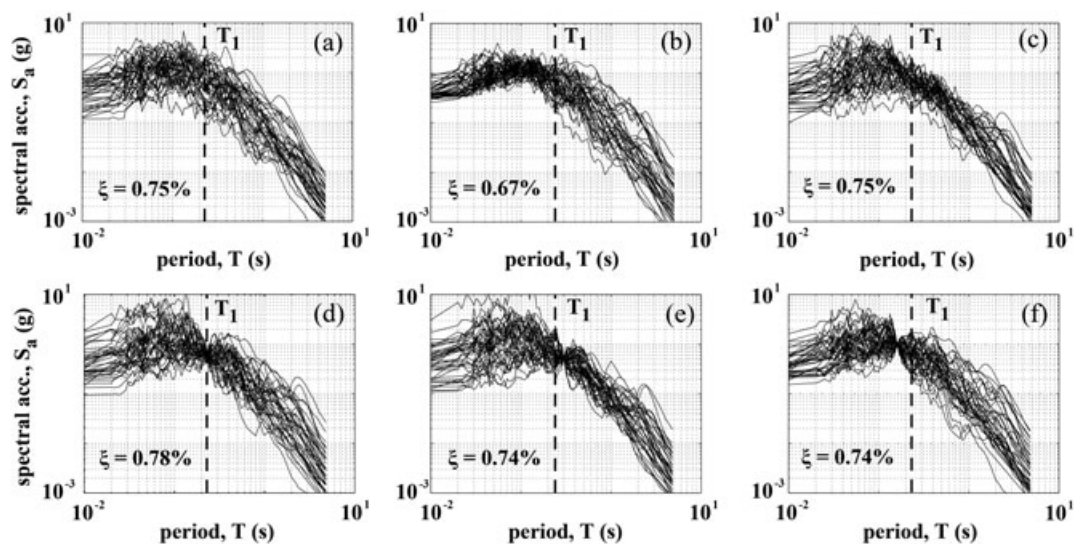


Figure 2. Linear-elastic acceleration response spectra,  $S_a$ , used in the study of Frame LE2: (a) GM[Uns]; (b) GM[ASCE7]; (c) GM[MIV]; (d) GM[ $S_a(T_1)$ ]; (e) GM[ $S_a(1.3 T_1)$ ]; (f) GM[ $S_a(0.7 T_1)$ ].

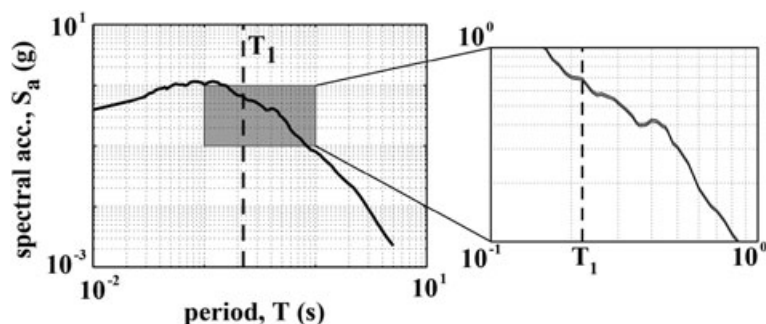


Figure 3. Median linear-elastic acceleration response spectra for the six suites in Figure 2.

only be viewed as representative findings. Note however that for short-to-medium period structures (about  $T_1 = 0.1\text{--}0.6$  s), even a small error in period estimation may have a similar effect as a larger error does because of the typically jagged characteristics of linear-elastic ground motion spectra in this period range.

In applying the ASCE-7 scaling method, the ground motions were scaled such that the average 5%-damped linear-elastic acceleration response spectrum for the suite was not less than the target median (geometric mean) spectrum of the unscaled records over the period range from 0.2 to 1.5 times the measured  $T_1$ . This scaling method utilized 5%-damped spectra (instead of the measured damping values) because this is a requirement dictated by ASCE-7. The median spectrum of the unscaled records rather than a code-based design spectrum was used as the target so as not to introduce a bias to the study. A different scaling factor was determined for each record in the GM[ASCE7] suite to minimize the SRSS error between the spectrum of the scaled record and the target spectrum within the period range of  $0.2T_1$  to  $1.5T_1$ . As stated previously, the ASCE-7 method does not provide any specific guidelines to result in a unique set of scaling factors for the records; various combinations of scaling factors can be found to satisfy the requirement that the average spectrum of the scaled records remains above the target spectrum over the specified period range. An algorithm, given in Appendix A of Kalkan and Chopra [18], was used in determining the scaling factors for the GM[ASCE7] suites in this paper.

The median (geometric mean) value of the scaling factors for the ground motions in each of the six suites from Figure 2 was 1.000, 0.996, 1.000, 0.976, 0.995, and 0.965 for GM[Uns], GM[ASCE7], GM[MIV], GM[ $S_d(T_1)$ ], GM[ $S_d(1.3T_1)$ ], and GM[ $S_d(0.7T_1)$ ], respectively. The resulting median response spectrum of the ground motions in each suite is depicted in Figure 3, where it can be seen that the median spectra of the different suites are essentially identical to one another (the small differences between the different median spectra are indistinguishable in Figure 3), only slightly varying in magnitude by at most 3% (in other words, the different scaling methods affect the details of the individual records while the median intensity is preserved).

## 5. TEST STRUCTURES

As shown in Figure 4(a), the frame structure configuration selected for the experimental investigation was a six-story, single-bay system with center-to-center span length of 762 mm and story height of 432 mm. These dimensions correspond to a building length scale of approximately  $S_L = 1/10$ . The structure was subjected to the six ground motion suites described previously with a time-scale of  $S_T = 1/3$ . The tests were conducted on a medium-sized uniaxial shake table that consists of a hydraulic actuator/servo-valve assembly and a hydraulic power supply that drives a  $1.2 \times 1.2$  m<sup>2</sup> slip table. Four different structure periods were investigated by varying the amount of superimposed mass on the test frame as follows (using 21-kg steel mass plates attached to the midspan of each beam):

- Frame LE1 - one superimposed mass plate at each floor and roof level;
- Frame LE2 - two mass plates at each floor and one plate at the roof;
- Frame LE3 - three mass plates at each floor and one plate at the roof;
- Frame LE4 - four mass plates at each floor and one plate at the roof.

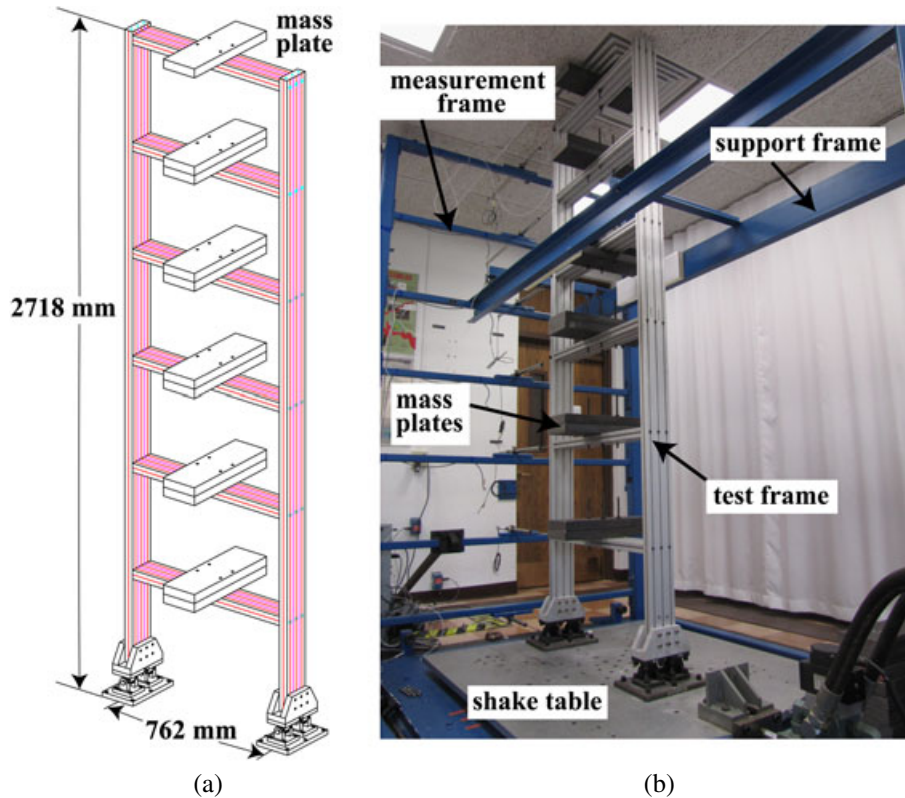


Figure 4. Frame LE2: (a) schematic; (b) test setup.

Figure 4(b) depicts Frame LE2 placed on the shake table, together with the measurement and out-of-plane support frames mounted onto the laboratory floor. The test frame was fabricated from extruded aluminum 6105-T5 alloy with a yield strength of  $241 \text{ MN/m}^2$ . The beam and column member cross sections were determined to result in stiffness appropriate with the scale model and with adequate strength to prevent yielding. The extruded aluminum cross section in Figure 5(a), oriented in the weak direction (with moment of inertia,  $I=295,524 \text{ mm}^4$  and area,  $A=1935 \text{ mm}^2$ ) was used for all beam and column members. To achieve a modular structure, each beam–column connection was constructed using three high-strength bolts passing through the column and screwing into holes tapped into the beam cross section at each end. The column bases were constructed with pinned connections. Figure 5(b) depicts a close-up view of the pinned base connection, which consists of a steel plate bolted to the shake table top, two steel clevises bolted to the plate, and two steel eye brackets inserted into the clevises and bolted to an aluminum fixture at the column base. A tight tolerance greased steel pin was used through the eye bracket-to-clevis connection to reduce friction while eliminating backlash effects.

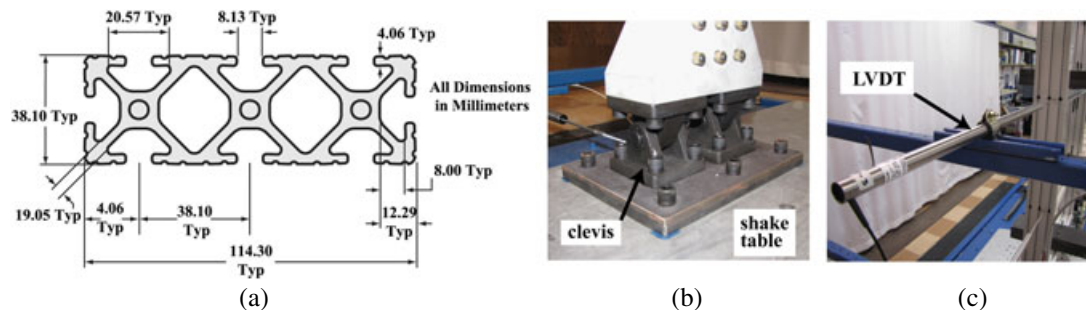


Figure 5. Test details: (a) extrusion profile for beam and column members (courtesy 80/20<sup>®</sup> Inc.); (b) pinned connection at column base; (c) linear variable differential transformer mounted to measurement frame.

Two accelerometers were used to monitor the in-plane lateral accelerations of the beam midspan at the roof and fourth floor level of the structure, and one additional accelerometer was placed directly on the shake table. In addition to the table in-plane lateral displacements, the displacements of the test structure were measured using seven free unguided linear variable differential transformers (LVDTs) (six at the floor and roof levels and one at the base) anchored between the structure and a fixed measurement frame. A mounted LVDT can be seen in Figure 5(c). The clamps used to attach the LVDTs to the measurement frame were engineered to mitigate vibrations. The data was collected at a high sampling rate (200 Hz), resulting in close-to-simultaneous excitation and response measurements.

## 6. BEHAVIOR OF TEST STRUCTURE UNDER STATIC LOADING

To determine the lateral load versus displacement behavior of the test structure under static loading, monotonic and reversed-cyclic pushover experiments were conducted by holding the fourth floor of the frame stationary while slowly displacing the base using the shake table. At the fourth floor level, a steel rod with pin-ended connections [Figure 6(a)] was placed between the test structure and a relatively stiff steel reaction frame. As the base of the structure was displaced, the resulting fourth floor force in the pin-ended rod was measured using an intermediary load cell. Two string potentiometer transducers were used to measure the absolute (i.e., with respect to a fixed reference) lateral displacements at the base and fourth floor level of the structure (note that the fourth floor displacements were very small but not zero because of the deformations of the reaction frame).

The fourth floor lateral force versus relative (with respect to the base) displacement behavior of the frame during two cycles of loading is shown using the thin black lines in Figure 6(b). The structure exhibited consistent and repeatable behavior in both the positive and negative loading directions, with a small amount of nonlinearity beginning at approximately 13 mm relative displacement. The nonlinear behavior occurred as the beam ends lost full contact with the columns due to the elongation of the beam–column connection bolts. The flexibility of the connection bolts also reduced the initial linear-elastic lateral stiffness of the frame (i.e., the beam–column connections were not perfectly rigid).

## 7. DYNAMIC CHARACTERISTICS OF TEST FRAMES

The dynamic characteristics of Frames LE1, LE2, LE3, and LE4 were measured by subjecting the structures to a series of sine-sweep tests. The results from three series of sine-sweep tests on Frame LE2 with base excitation amplitudes ranging from 0.13 to 0.38 mm can be seen in Figure 7(a), where the  $y$ -axis shows the ratio of the relative roof displacement amplitude to the base excitation displacement amplitude, and the  $x$ -axis shows the frequency of the sine wave exciting the structure. Although some dependency on the displacement amplitude was observed in the results, the fundamental frequencies were found as  $f_1 = 5.32, 4.35, 3.82,$  and  $3.42$  Hz for Frames LE1, LE2, LE3, and LE4, respectively (corresponding to periods of  $T_1 = 0.19, 0.23, 0.26,$  and  $0.29$  s, respectively). With the selected time-scale of  $S_T = 1/3$ ,

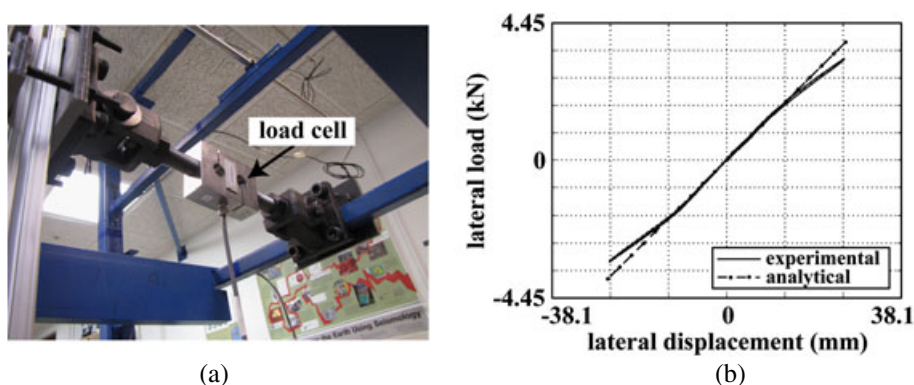


Figure 6. Static tests: (a) load cell assembly; (b) fourth floor lateral load versus relative displacement behavior.

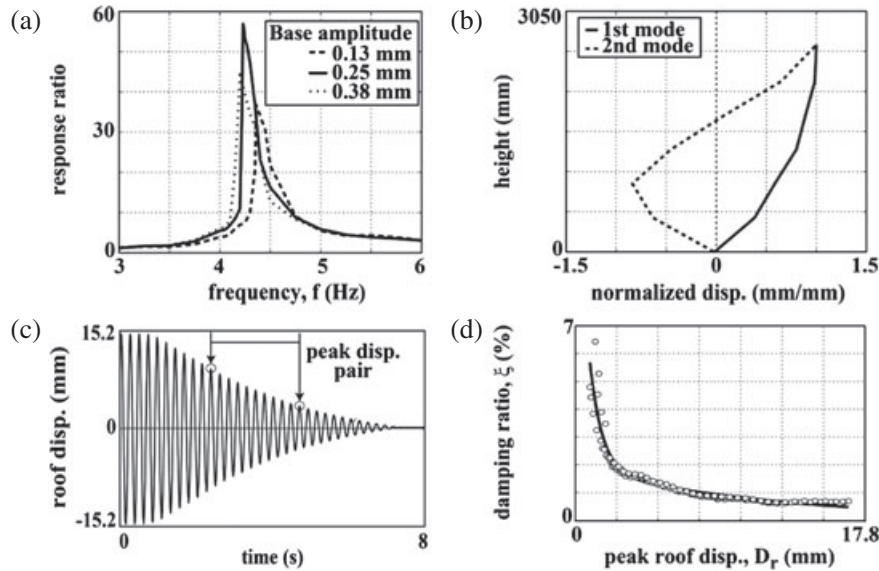


Figure 7. Dynamic characteristics of Frame LE2: (a) resonance peaks; (b) first and second mode shapes; (c) decay of roof displacement response; (d) displacement-dependent damping.

the test specimens correspond to full-scale structures with fundamental periods of  $T_1 = 0.56, 0.69, 0.79,$  and  $0.88$  s, respectively. The measured mode shapes for Frame LE2 in the first two modes of vibration can be seen in Figure 7(b).

The damping ratio for each structure was determined using the logarithmic decrement method [40] on the decay of the measured relative roof displacement response. The logarithmic decrement method was applied to a series of peak roof displacement pairs with decreasing amplitudes, each pair 10 cycles apart as shown on the typical roof displacement time-history for Frame LE2 in Figure 7(c). As can be seen in Figure 7(d), a correlation was evident between the amplitude of the peak relative roof displacement and the amount of damping exhibited by the structure. For use in the dynamic response history analyses described later and in determining the scaling factors for the  $S_d(T_1)$ ,  $S_d(1.3 T_1)$ , and  $S_d(0.7 T_1)$  methods, a displacement-dependent damping regression line [e.g., solid line in Figure 7(d)] was fit to the data for each structure (slight differences were observed in the damping regression lines for the four test frames).

## 8. ANALYTICAL MODELING

For the purposes of the analytical component of the research, models of the test structures were developed using the OpenSees [41] program. The extruded aluminum cross section in Figure 5(a) was modeled using fiber cross sections for the beam and column members. The column bases were modeled as pinned, and the flexibility of the beam–column connections (due to the flexibility of the connection bolts) was modeled by placing linear-elastic zero-length rotational springs at the beam ends as shown in Figure 8. The stiffness of the rotational springs was determined by calibrating the model results [dashed-dotted line in Figure 6(b)] with the linear-elastic range of the measured lateral load versus displacement behavior of the structure.

Modal analyses of the models showed excellent comparisons with the measured first mode shapes and frequencies of the test structures. In addition, RHA results were compared with measured response histories. For example, analytical and measured roof displacement response comparisons for Frame LE2 under two unscaled ground motion records from Table I can be seen in Figure 9. Once the accuracy of the analytical results was deemed sufficient, the OpenSees model was integrated with a MATLAB<sup>®</sup> script to subject the structures to the six suites of ground motions and to guide the shake table tests described in the next section. A slightly different damping ratio was used for each structure analyzed under each ground motion suite, as determined from the displacement-dependent damping regression line [e.g., solid line in Figure 7(d)] at the median peak roof displacement of the structure under that suite.

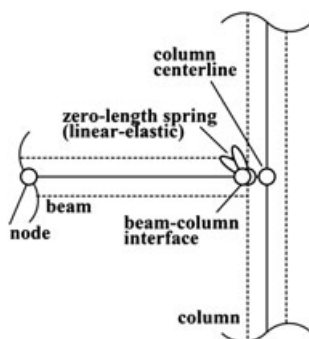


Figure 8. Analytical modeling of beam–column joints.

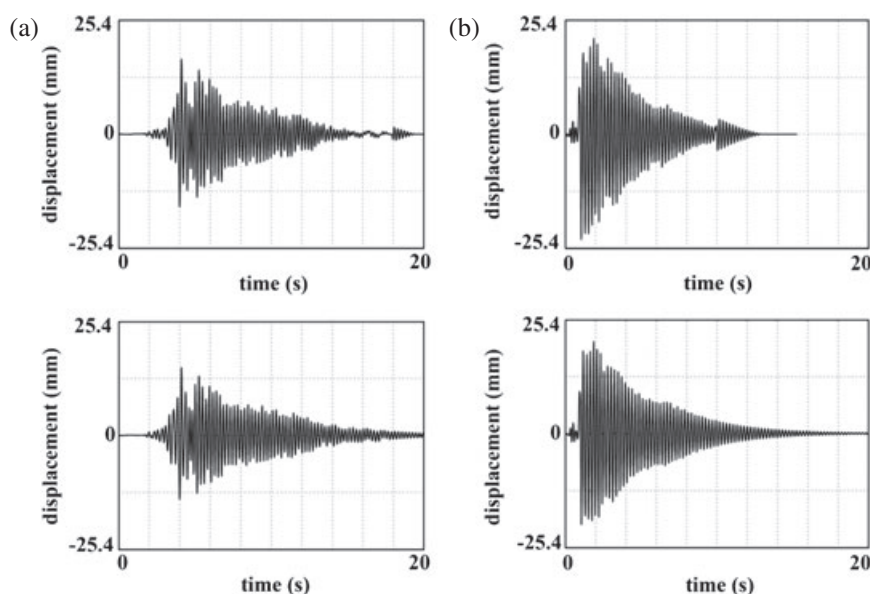


Figure 9. Measured (top) and analytical (bottom) roof displacement responses of Frame LE2: (a) STG000; (b) CPM000.

## 9. EFFECT OF GROUND MOTION SCALING

With the characteristics of Frames LE1, LE2, LE3, and LE4 determined and the expected displacement demands from the ground motions in each suite estimated by the calibrated analytical models, the test specimens were subjected to a series of shake table experiments. For each structure, the pre-test analyses indicated that several ground motions were likely to subject the frame through significant nonlinear displacements. To avoid damaging the specimen, these ground motions were excluded from the experimental investigation (but kept for the analytical study), resulting in 25 records that were common to the testing of the four structures (gray shaded rows in Table I). The peak roof drift ( $\Delta_r$ ) demands from the six series of tests for each structure are plotted in Figure 10. It can be seen that the  $\Delta_r$  demands from the GM[Uns] suite (■ markers) are not as strongly correlated to  $MIV$  as compared with the correlation to  $S_a$ . Note that the  $S_a$  values in Figure 10 are plotted at  $T_1$  for the GM[Uns], GM[ASCE7], and GM[ $S_a(T_1)$ ] suites, and at  $0.7 T_1$  and  $1.3 T_1$  for the GM[ $S_a(0.7 T_1)$ ] and GM[ $S_a(1.3 T_1)$ ] suites, respectively.

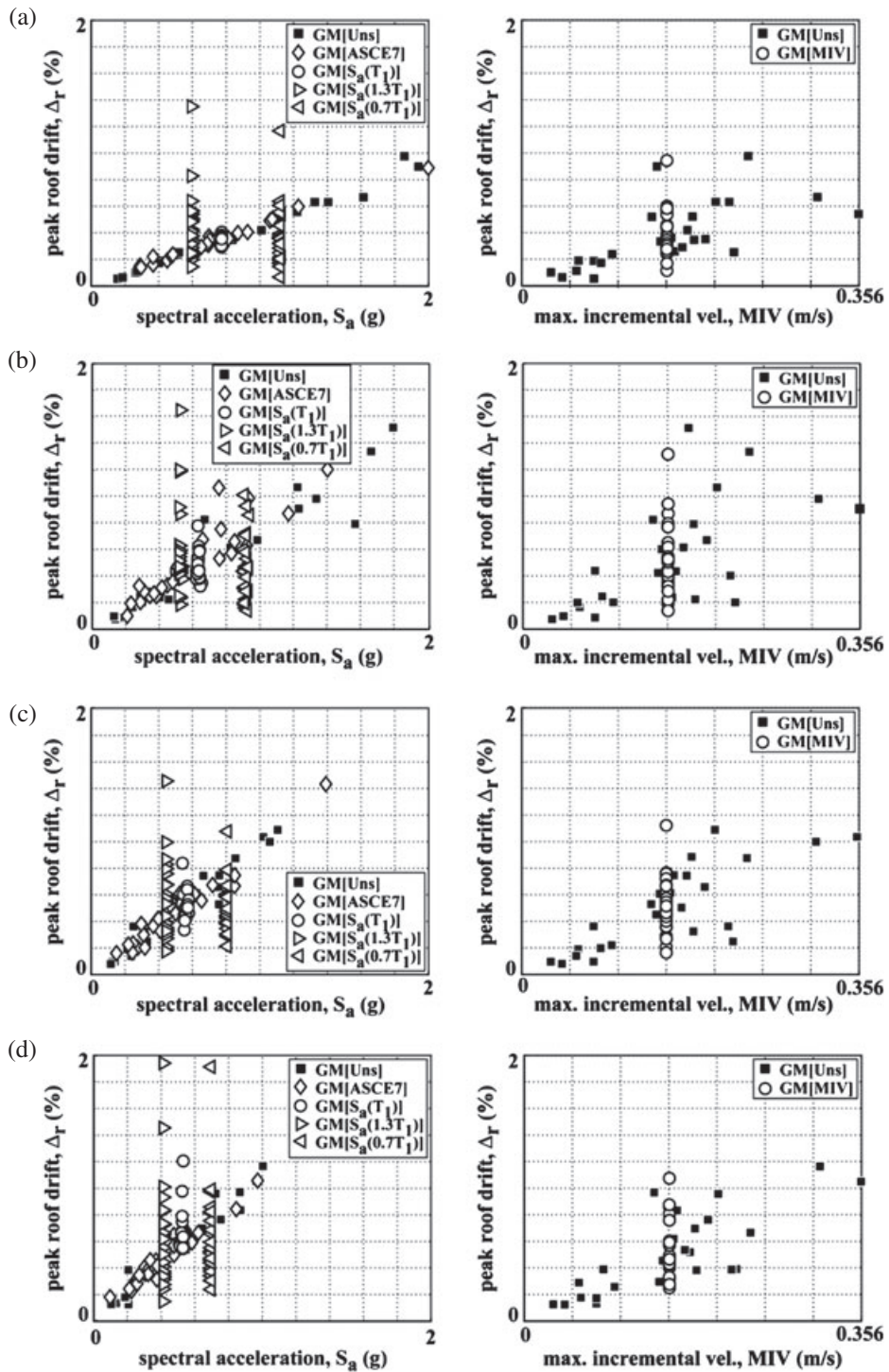


Figure 10. Peak roof drift,  $\Delta_r$  demands plotted against  $S_a$  and MIV: (a) Frame LE1; (b) Frame LE2; (c) Frame LE3; (d) Frame LE4.

The resulting median peak roof drift demand,  $\hat{\Delta}_r$ , and the coefficient of variation (COV) of the peak roof drift demands for Frames LE1, LE2, LE3, and LE4 under each ground motion suite are listed in Table II (note that in addition to the test frames, Table II includes results from the analytical study described in the next section). The COV measure, defined as the ratio between the sample standard deviation and the

Table II. Summary results for peak roof drift demands.

$T_1$ (s)	GM[Uns]		GM[ASCE7]		GM[MIV]		GM[ $S_a(T_1)$ ]		GM[ $S_a(1.3T_1)$ ]		GM[ $S_a(0.7T_1)$ ]	
	$\hat{\Delta}_r$ (%)	COV( $\Delta_r$ )										
0.15	0.33	0.66	0.30	0.41	0.37	0.41	0.29	0.08	0.29	0.44	0.26	0.56
0.19 (LE1)	0.35	0.64	0.31	0.47	0.35	0.45	0.35	0.09	0.41	0.57	0.32	0.63
0.23 (LE2)	0.44	0.75	0.45	0.59	0.45	0.53	0.44	0.23	0.48	0.56	0.44	0.53
0.26 (LE3)	0.50	0.62	0.42	0.56	0.52	0.39	0.54	0.18	0.44	0.56	0.50	0.35
0.29 (LE4)	0.45	0.59	0.41	0.79	0.49	0.39	0.63	0.22	0.62	0.62	0.51	0.58
0.43	0.86	0.61	0.89	0.51	1.00	0.44	0.99	0.07	0.94	0.54	1.26	0.37
0.53	0.95	0.56	1.03	0.52	1.21	0.42	1.03	0.08	1.24	0.47	1.09	0.38
0.66	0.73	0.71	0.76	0.64	0.86	0.54	0.91	0.13	0.99	0.29	0.81	0.55
0.81	0.62	0.69	0.80	0.43	0.80	0.45	0.90	0.19	0.88	0.49	0.80	0.34
1.00	1.02	0.65	1.13	0.61	0.97	0.53	1.06	0.16	1.19	0.46	1.17	0.59

Notes: 1) The results for Frames LE1, LE2, LE3, and LE4 are test data.  
2) MIV method performs as well as or better than the results in shaded cells.

sample mean, is used to assess the effectiveness of the scaling methods in reducing the dispersion in  $\Delta_r$ . As can be expected for a linear-elastic structure, the  $S_a(T_1)$  scaling method produced the smallest dispersion in  $\Delta_r$ . However, the dispersion more than doubled when a 30% error was introduced in period estimation, resulting in values greater than the dispersion from the MIV-scaled suite for most of the cases studied (gray shaded cells in Table II). Further, with the exception of one case ( $T_1 = 0.81$  s), the MIV method performed as well as or better than the ASCE-7 method with regard to minimizing dispersion.

These results are important in showing that, for linear-elastic systems, inaccuracies in the estimation of a structure's fundamental period can lead to a much larger dispersion in the seismic demand estimates for the  $S_a(T_1)$  scaling method when compared with the dispersion achieved with the records scaled on the basis of the 'exact' period. The MIV scaling method, which is not dependent on the properties of the structure, resulted in a simpler procedure while also producing less uncertainty in the estimated seismic demands for many of the cases studied. The ASCE-7 method was the least consistent and least effective in reducing the dispersion in the  $\Delta_r$  demands of the four test structures, exhibiting a wide COV range from 0.47 to 0.79. For Frame LE4, the dispersion resulting from the ASCE-7 method even surpassed that of the unscaled suite.

## 10. ANALYTICAL EXTENSION OF RESULTS

This section uses the validated analytical models of the test frames to extend the shake table results over a wider range of parameters. First, the superimposed floor and roof masses of the analytical model were varied to result in a series of 10 six-story analytical structures with fundamental periods exponentially spaced between  $T_1 = 0.15$  and 1.00 s. As shown in Table II, four of the selected periods matched the measured periods of Frames LE1 through LE4 for the validation of the results. This analytical period range, which corresponds to full-scale structural periods of 0.45–3.00 s, is representative of a much wider range of buildings, including short and long period structures. To keep the comparisons in Table II consistent, the structures were analyzed using the same 25 records that were common to the testing of Frames LE1–LE4 (gray shaded rows in Table I). As depicted in Figure 11, the dispersion in the resulting  $\Delta_r$  demands can be visualized as COV spectra from each ground motion suite. Consistent with the results in Figure 10, the dispersion from the  $S_a(T_1)$  scaling method (\* markers in Figure 11) outperformed the other scaling methods throughout the entire range of periods. The unscaled suite (thick solid line with  $\square$  markers) produced the largest dispersion in  $\Delta_r$  for nine of the 10 structures, with the GM[ASCE7] (thick dotted line with  $\diamond$  markers), GM[ $S_a(1.3T_1)$ ], GM[ $S_a(0.7T_1)$ ], and GM[MIV] (thick dashed line with  $\Delta$  markers) suites producing, on average, less dispersion in order of improved performance. These results confirm the potential vulnerabilities of structure-dependent ground motion scaling methods for use in linear-elastic RHA

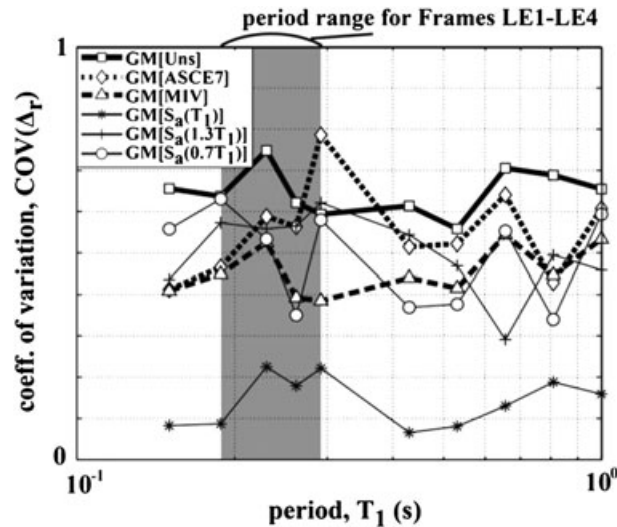


Figure 11.  $COV(\Delta_P)$  over a range of periods (Note: results for Frames LE1, LE2, LE3, and LE4 are test data).

over a wider range of structure periods. Note that the results presented in Table II and Figure 11 for Frames LE1, LE2, LE3, and LE4 are test data, whereas the other results were obtained from analytical simulations. The  $COV(\Delta_P)$  values obtained from the test data under the  $GM[S_a(T_1)]$  suite were generally larger than the values obtained from the corresponding analytical simulations. The cause of this difference is not known; however, it could be due to the sensitivity of the  $S_a(T_1)$  scaling method to the exact properties of the structure, which were difficult to model accurately (e.g., any nonlinear behavior at the pinned base of the specimen). Although these differences between the experimental and analytical results do exist, they do not detract from the overall observations presented herein.

As a second analytical study, the six-story OpenSees model was extended to one-story, four-story, and 14-story structures. The complete suite of 39 ground motion records was used in this study because, unlike the physical test specimens, the analytical models could be made to behave linear elastically under all of the records. The superimposed mass was held constant at two mass plates per floor and one plate on the roof, resulting in fundamental periods of  $T_1 = 0.047, 0.16, 0.23,$  and  $0.52$  s for the one-story, four-story, six-story, and 14-story structures, respectively (corresponding to full-scale periods of 0.14, 0.47, 0.69 and 1.55 s, respectively). The focus of the study was the ‘accuracy’ of the ground motion scaling methods (that is, ability to provide accurate estimates of the median peak demands as if a much larger set of records were used). Thus, for each structure and scaling method, nine subset ground motion bins were selected, each bin containing seven records from the full set of 39 records. Note that the use of seven ground motions in each bin is consistent with the ASCE 7–10 requirements.

Bins 1–3 were chosen randomly from the full set, but a bias was introduced into the remaining six subsets. For these subsets, Bins 4–6 were selected with a weak ground motion bias and Bins 7–9 were selected with a strong ground motion bias. To introduce this bias, the 39 ground motions were sorted by ascending peak roof drift demand for each structure and scaling method, and the records were either selected from below the median roof drift to introduce a weak bias or from above the median drift to introduce a strong bias.

The accuracy of the scaling methods was evaluated using the inter-story drift ratio,  $r(\hat{\delta})$ , defined as the ratio between the median inter-story drift demand,  $\hat{\delta}_s$  from each subset ground motion bin and the benchmark demand determined as the median inter-story drift demand,  $\hat{\delta}_b$  from the full unscaled suite of 39 ground motions. The dispersion in the peak inter-story drift demands,  $COV(\delta)$  was also calculated for each ground motion bin. The variation in  $r(\hat{\delta})$  and  $COV(\delta)$  over the height of the six-story frame can be seen in Figures 12 and 13, respectively.

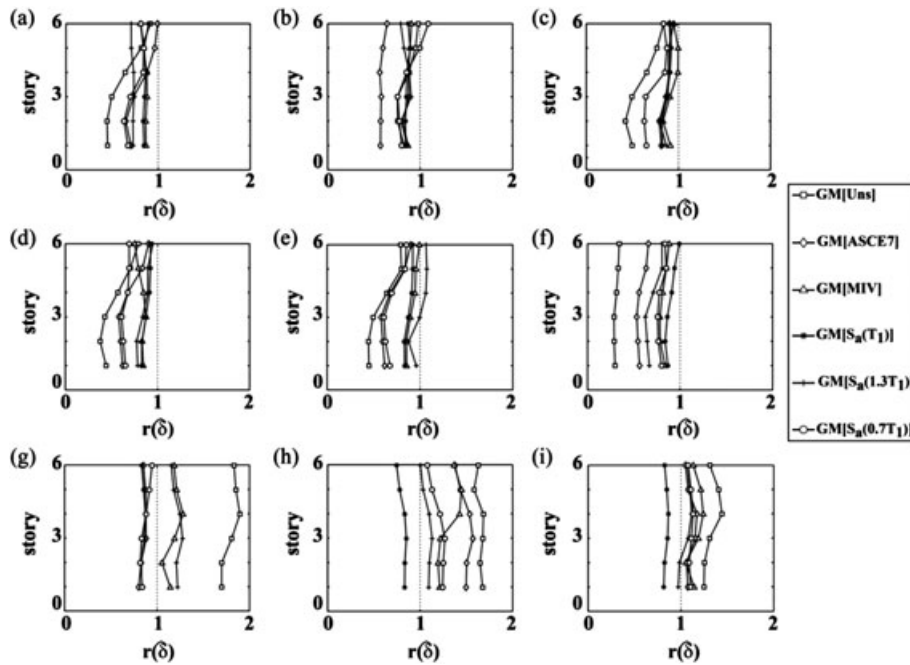


Figure 12. Inter-story drift ratio,  $r(\hat{\delta})$  for the six-story frame: (a)–(i) Bins 1–9.

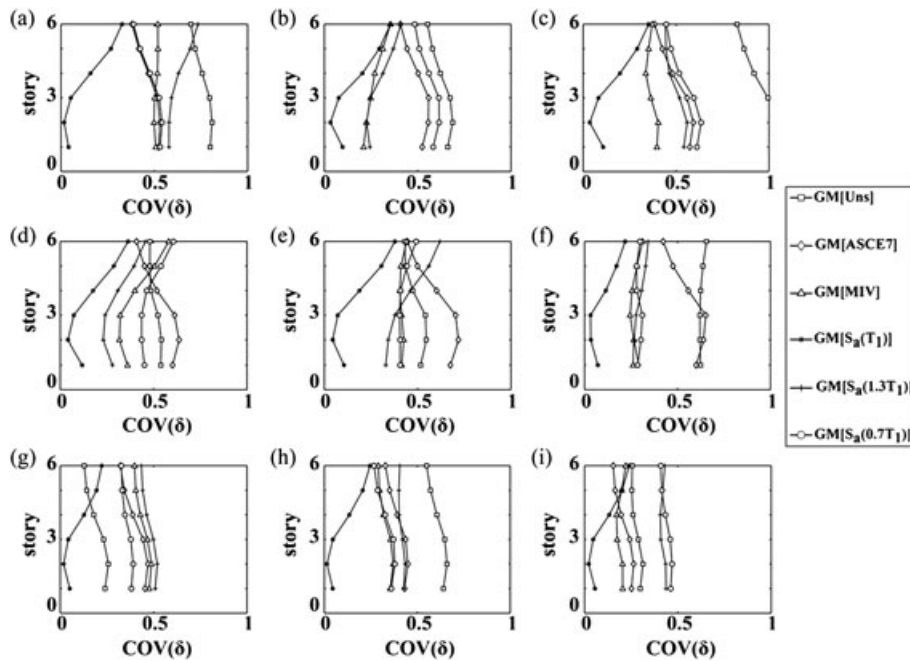


Figure 13. Dispersion in inter-story drift demands,  $COV(\delta)$  for the six-story frame: (a)–(i) Bins 1–9.

In Figure 12,  $r(\hat{\delta}) = 1$  indicates perfect accuracy where the median inter-story drift from the subset bin,  $\hat{\delta}_s$  matches that of the benchmark full suite of unscaled ground motions,  $\hat{\delta}_b$ . As an overall measure of accuracy, the average absolute error in the median inter-story drift  $|\bar{E}(\hat{\delta})|$  was calculated for each bin by dividing the sum of the absolute error,  $|E(\hat{\delta})| = |r(\hat{\delta}) - 1|$  for each story by the number of stories.

Similarly, the average dispersion in the inter-story drift was calculated as  $\overline{\text{COV}}(\delta)$ . Finally, to determine whether a scaling method was more likely to overestimate or underestimate the median demands, the maximum and minimum errors,  $E_m(\hat{\delta}) = \max$  and  $\min[r(\hat{\delta}) - 1]$  in the median inter-story drift demands over the height of each structure were also calculated. Positive  $E_m(\hat{\delta})$  values indicate an overestimation of the median drift relative to the benchmark demand, possibly leading to an uneconomical design. Conversely, negative values of  $E_m(\hat{\delta})$  represent an unconservative underestimation of the median demand.

The  $|\overline{E}(\hat{\delta})|$ ,  $\overline{\text{COV}}(\delta)$ , and  $E_m(\hat{\delta})$  results for the one-story, four-story, six-story, and 14-story structures are plotted as bar graphs in Figures 14, 15, and 16, respectively (note that the data from a few of the analysis cases for the one-story frame extend outside the plotted range of the graphs as annotated in the figures). All three sets of plots should be considered in evaluating the scaling methods. For example, looking at Figure 15(c) for the six-story frame, the  $\overline{\text{COV}}(\delta)$  value under Bin 7 from the unscaled suite is relatively small (indicating low dispersion in the inter-story drift demands). However, the  $|\overline{E}(\hat{\delta})|$  and  $E_m(\hat{\delta})$  values for the same bin are very large [Figures 14(c) and 16(c)], indicating poor accuracy in the results.

Although there is considerable variability in the results between the different bins, Figures 14–16 are consistent with the previous finding that, on average, the  $S_a(T_1)$  scaling method is more effective in minimizing bin dispersion,  $\overline{\text{COV}}(\delta)$ , and error,  $|\overline{E}(\hat{\delta})|$  and  $E_m(\hat{\delta})$ . To further analyze and condense the results from Figures 14 and 15, Table III shows the average (i.e., mean value of the nine analysis bins for a given structure and scaling method) and maximum (i.e., maximum value from the nine bins for a given structure and scaling method)  $|\overline{E}(\hat{\delta})|$  and  $\overline{\text{COV}}(\delta)$ . Table III also shows the maximum absolute  $E_m(\hat{\delta})$  from Figure 16 (i.e., maximum value in magnitude over the nine bins) to demonstrate potentially dramatic deviations of the median bin inter-story drifts from the benchmark full suite median inter-story drifts. The increased error and dispersion for the  $S_a(1.3T_1)$  and  $S_a(0.7T_1)$  methods reinforce that inaccuracies in period estimation can considerably erode the effectiveness of the  $S_a(T_1)$  method. Comparisons between the *MIV*, *ASCE-7*,  $S_a(1.3T_1)$ , and  $S_a(0.7T_1)$  results are mixed and no statistically significant argument applicable to all the cases studied can be made. However, as depicted by the gray shaded cells in Table III, the *MIV* method provides better performance in minimizing the bin dispersion and error for most of the cases studied, except for the

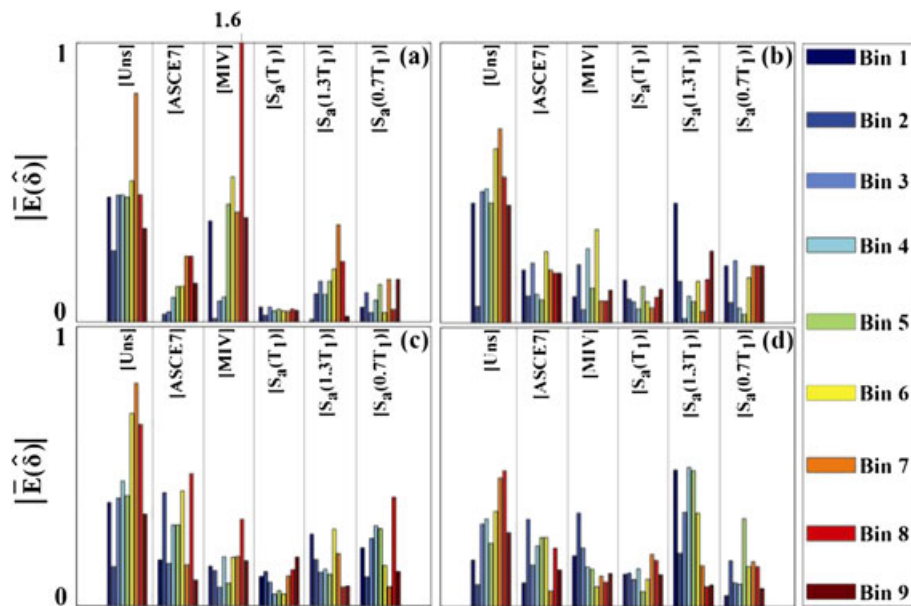


Figure 14. Average absolute error in median inter-story drift demands,  $|\overline{E}(\hat{\delta})|$  for Bins 1–9: (a) one-story frame; (b) four-story frame; (c) six-story frame; (d) 14-story frame.

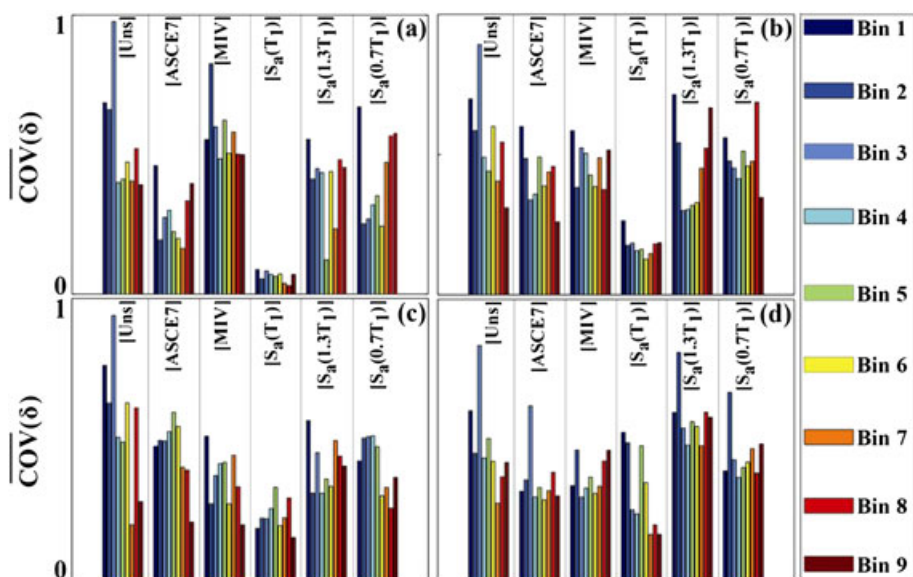


Figure 15. Average dispersion in inter-story drift demands,  $\overline{\text{COV}}(\hat{\delta})$  for Bins 1–9: (a) one-story frame; (b) four-story frame; (c) six-story frame; (d) 14-story frame.

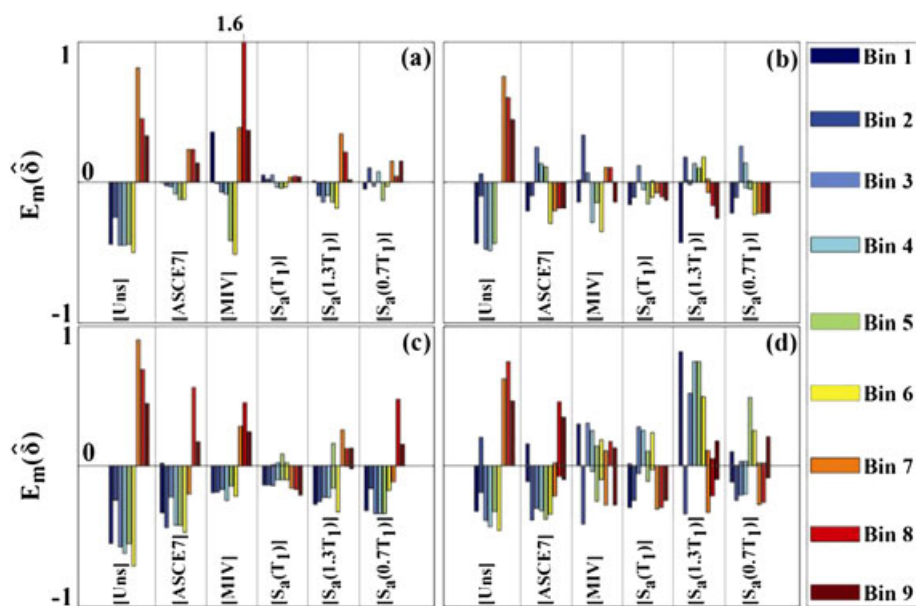


Figure 16. Maximum and minimum errors in median inter-story drift demands,  $E_m(\hat{\delta})$  for Bins 1–9: (a) one-story frame; (b) four-story frame; (c) six-story frame; (d) 14-story frame.

one-story frame. Because short period structures are less affected by the impulsive characteristics of a ground motion, it should be expected that the *MIV* scaling method is not effective for the one-story frame. Additional statistical studies, such as the Student's *t*-tests [38], were conducted as part of a more quantitative comparison on the performance differences between the scaling methods, supporting the over-arching conclusions presented herein (see Appendix for sample *t*-test results).

Note that although ASCE-7 requires scaling on the basis of a range of structural periods [rather than only the fundamental period as required for the  $S_a(T_1)$  method], this period range is still based on an estimate of the fundamental period thus making the ASCE-7 scaling method susceptible to similar shortcomings as the  $S_a(T_1)$  method. In other words, uncertainties and approximations in the modeling

Table III. Summary results for  $|\bar{E}(\hat{\delta})|$ ,  $\overline{\text{COV}}(\delta)$ , and  $E_m(\hat{\delta})$ .

Scaling Method	$ \bar{E}(\hat{\delta}) $								$\overline{\text{COV}}(\delta)$								$E_m(\hat{\delta})$			
	1-Story		4-Story		6-Story		14-Story		1-Story		4-Story		6-Story		14-Story		1-St.	4-St.	6-St.	14-St
	Avg	Max	Avg	Max	Avg	Max	Avg	Max	Avg	Max	Avg	Max	Avg	Max	Avg	Max	Max	Max	Max	Max
GM[Uns]	0.46	0.82	0.45	0.69	0.47	0.80	0.29	0.49	0.55	0.98	0.55	0.89	0.56	0.94	0.48	0.84	0.82	0.75	0.90	0.74
GM[ASCE7]	0.11	0.23	0.16	0.25	0.28	0.49	0.19	0.32	0.28	0.46	0.43	0.61	0.47	0.61	0.36	0.64	0.23	0.29	0.57	0.46
GM[MIV]	0.43	1.60	0.15	0.33	0.16	0.31	0.16	0.34	0.57	0.83	0.47	0.59	0.36	0.51	0.37	0.47	1.60	0.35	0.45	0.42
GM[ $S_a(T_1)$ ]	0.04	0.05	0.06	0.09	0.14	0.19	0.10	0.20	0.06	0.09	0.07	0.10	0.15	0.18	0.31	0.61	0.05	0.11	0.25	0.34
GM[ $S_a(1.3T_1)$ ]	0.14	0.35	0.18	0.36	0.16	0.29	0.31	0.51	0.40	0.55	0.47	0.77	0.42	0.64	0.60	0.87	0.35	0.41	0.38	0.84
GM[ $S_a(0.7T_1)$ ]	0.08	0.15	0.22	0.34	0.21	0.34	0.19	0.40	0.41	0.67	0.54	0.61	0.44	0.56	0.48	0.59	0.15	0.36	0.39	0.77

Note: *MIV* method outperforms the results in shaded cells.

and analysis of the structure (e.g., damping and period) make the design application of the ASCE-7 and  $S_a(T_1)$  methods more uncertain than the application of the *MIV* method. With the exception of structures with very short fundamental periods (e.g., the one-story frame in this investigation), it may be more advantageous to use the *MIV* method, which is structure-independent and can be applied to a ground motion suite without the need to estimate the properties of the structure. Further, any changes in the structure properties would not require the scaling of the ground motions to be iterated. The biggest disadvantage for the implementation of the *MIV* scaling method in seismic design is the lack of methods to estimate the mean annual frequency of exceedence of *MIV* and methods to estimate the attenuation of *MIV* [15]. Thus, there is currently no accepted method to determine the probability of exceedence of a certain *MIV* level at a given site. Future research is needed in these areas before the *MIV* scaling method can be used in design practice.

## 11. SUMMARY AND CONCLUSIONS

This paper describes an integrated experimental and analytical evaluation of selected ground motion scaling methods for use in dynamic response history analysis of building frame structures exhibiting no or limited nonlinearity. The general experimental setup and features of a 1/10-scale six-story linear-elastic test frame specimen are presented, along with the identification of the static and dynamic properties of the structure. The scaling methods are evaluated by determining the dispersion in the peak lateral drift demands of the structures as well as the accuracy in the median demands when a smaller subset of ground motions is used, including the effects of biased selection of these subsets. Analytical parameter studies are conducted to extend the applicability of the experimental results over a wider range of building properties. The results and findings are limited to the structures, demand parameters, and ground motion records investigated.

As can be expected, the  $S_a(T_1)$  scaling method is the most effective in minimizing dispersion and maximizing accuracy in the seismic drift demands for linear-elastic structures. However, inaccuracies in the estimation of the structure fundamental period,  $T_1$  can significantly erode this effectiveness as demonstrated by the comparatively poor performance of the  $S_a(1.3T_1)$  and  $S_a(0.7T_1)$  methods. For structures with limited or no nonlinearity, these results reinforce the potential uncertainty that can arise from scaling methods that require design estimations for the fundamental period. Comparisons between the *MIV*, ASCE-7,  $S_a(1.3T_1)$ , and  $S_a(0.7T_1)$  results are mixed and no statistically significant argument applicable to all the cases studied can be made. However, with the exception of structures with very short periods, the *MIV* method is shown to provide better performance in minimizing dispersion and maximizing accuracy in the lateral drift demands for most of the cases studied in this paper. The increased dispersion produced by the *MIV* method for the one-story structure demonstrates that this method may not be suitable for structures with fundamental periods that are significantly different from the impulsive characteristics of the ground motion records in the suite. Because the *MIV* scaling method is structure-independent, it can be applied without the need to estimate the fundamental period of the structure being designed, and any changes in the building properties would not require the scaling of the ground motions to be iterated.

APPENDIX A: REPRESENTATIVE STUDENT'S *T*-TEST RESULTS

The statistical significance of the performance differences between the different scaling methods can be evaluated by comparing the means of the corresponding data sets on the basis of the Student's *t*-test [38]. Tailed *t*-tests were performed on the results from the study in Figure 11 as well as the results from the study in Figures 14–16 to evaluate the scaling methods with respect to accuracy and efficiency. This evaluation was conducted using the *p*-values generated from the *t*-tests to quantify whether the mean of the data corresponding to one scaling method was statistically greater than the mean of the data corresponding to another scaling method.

Indicative results are presented in Tables A1 and A2 showing the *p*-values from the  $\overline{\text{COV}}(\delta)$  data (average dispersion in the inter-story drift) for the one-story and six-story structures in Figure 15(a) and (c), respectively. In these tables, a *p*-value less than the generally accepted threshold of 5% (gray shaded cells) indicates that the scaling method corresponding to that column statistically performed significantly better than the scaling method corresponding to that row (i.e., the null hypothesis can be rejected at the 5% significance level for that method-to-method comparison). It can be seen that the *MIV* scaling method does not outperform any of the other methods with statistical significance for the one-story (short period) structure; however, the effectiveness of the *MIV* method becomes more significant for the six-story structure, supporting the over-arching conclusions presented in the paper. The results for the six-story structure also reinforce that inaccuracies in period estimation [i.e., the  $S_a(1.3T_1)$  and  $S_a(0.7T_1)$  methods] can considerably erode the effectiveness of the  $S_a(T_1)$  method.

Table A1. *T*-test *p*-values for the  $\overline{\text{COV}}(\delta)$  data for the one-story structure [Figure 15(a)].

Scaling Method	GM[Uns]	GM[ASCE7]	GM[MIV]	GM[ $S_a(T_1)$ ]	GM[ $S_a(1.3T_1)$ ]	GM[ $S_a(0.7T_1)$ ]
GM[Uns]	-	0.0002	0.0240	0.0003	0.0115	0.0010
GM[ASCE7]	0.9998	-	0.9851	0.0065	0.8768	0.8241
GM[MIV]	0.9760	0.0149	-	0.0034	0.1512	0.0326
GM[ $S_a(T_1)$ ]	0.9997	0.9935	0.9966	-	0.9824	0.9925
GM[ $S_a(1.3T_1)$ ]	0.9885	0.1233	0.8488	0.0176	-	0.2003
GM[ $S_a(0.7T_1)$ ]	0.9990	0.1759	0.9674	0.0075	0.7997	-

Note: Shaded cells indicate that the scaling method for that column statistically outperforms the method for that row.

Table A2. *T*-test *p*-values for the  $\overline{\text{COV}}(\delta)$  data for the six-story structure [Figure 15(c)].

Scaling Method	GM[Uns]	GM[ASCE7]	GM[MIV]	GM[ $S_a(T_1)$ ]	GM[ $S_a(1.3T_1)$ ]	GM[ $S_a(0.7T_1)$ ]
GM[Uns]	-	0.0967	0.0159	0.0002	0.0584	0.0561
GM[ASCE7]	0.9033	-	0.0120	0.0000	0.2444	0.2784
GM[MIV]	0.9841	0.9880	-	0.0001	0.9707	0.9462
GM[ $S_a(T_1)$ ]	0.9998	1.0000	0.9999	-	1.0000	1.0000
GM[ $S_a(1.3T_1)$ ]	0.9416	0.7556	0.0293	0.0000	-	0.6083
GM[ $S_a(0.7T_1)$ ]	0.9439	0.7216	0.0538	0.0000	0.3917	-

Note: Shaded cells indicate that the scaling method for that column statistically outperforms the method for that row.

## ACKNOWLEDGEMENTS

This research is funded by the National Science Foundation (NSF) under Grant No. CMMI 0928662. The support of Dr. M. P. Singh, former NSF Program Director, and Dr. K. I. Mehta, current NSF Program Director, is gratefully acknowledged. The authors would also like to acknowledge the following individuals: Paulo Bazzurro, University Institute for Superior Studies (IUSS); Brendon Bradley, University of Canterbury; Sigmund Freeman, Wiss, Janney, Elstner Associates, Inc.; Bob St. Henry, NEFF Engineering; Vladimir Graizer, U.S. Nuclear Regulatory Commission; Farzad Naeim, John A. Martin and Associates, Inc.; Thomas Sabol, Englekirk & Sabol Consulting Structural Engineers, Inc.; and Nilesh Shome, Risk Management Solutions. The opinions, findings, and conclusions presented in the paper are those of the authors and do not necessarily reflect the views of these organizations and individuals.

## REFERENCES

1. Kennedy R, Short S, Merz K, Tokarz F, Idriss I, Powers M, Sadigh K. Engineering characterization of ground motion-task I: effects of characteristics of free-field motion on structural response. NUREG/CR-3805, U.S. Regulatory Commission, Washington, D.C., 1984.
2. Nau J, Hall W. Scaling methods for earthquake response spectra. *Journal of Structural Engineering* 1984; **110**:91–109.
3. Miranda E. Evaluation of site-dependent inelastic seismic design spectra. *Journal of Structural Engineering* 1993; **119**(5):1319–1338.
4. Vidic T, Fajfar P, Fischinger M. Consistent inelastic design spectra: strength and displacement. *Earthquake Engineering and Structural Dynamics* 1994; **23**:507–521.
5. Martinez-Rueda J. Scaling procedure for natural accelerograms based on a system of spectrum intensity scales. *Earthquake Spectra* 1998; **14**:135–152.
6. Shome N, Cornell C. Probabilistic seismic demand analysis of nonlinear structures. Reliability of Marine Structures Program Report No. RMS-35, Department of Civil and Environmental Engineering, Stanford University, CA, 1999.
7. Baez J, Miranda E. Amplification factors to estimate inelastic displacement demands for the design of structures in the near field. *12th World Conference on Earthquake Engineering*, Auckland, New Zealand, Paper No. 1561, 2000.
8. Malhotra P. Strong-motion records for site-specific analysis. *Earthquake Spectra* 2003; **19**(3):557–578.
9. Naeim F, Alimoradi A, Pezeshk S. Selection and scaling of ground motion time histories for structural design using genetic algorithms. *Earthquake Spectra* 2004; **20**(2):413–426.
10. Luco N, Cornell A. Structure-specific scalar intensity measures for near-source and ordinary earthquake ground motions. *Earthquake Spectra* 2007; **23**(2):357–392.
11. Tothong P, Cornell A. Structural performance assessment under near-source pulse-like ground motions using advanced ground motion intensity measures. *Earthquake Engineering and Structural Dynamics* 2008; **37**(7):1013–1037.
12. Shome N, Cornell C. Normalization and scaling accelerograms for nonlinear structural analysis. *6th U.S. National Conf. on Earthquake Engin.*, Seattle, WA, CD-ROM, 1998.
13. Shome N, Cornell C, Bazzurro P, Carballo J. Earthquakes, records, and nonlinear responses. *Earthquake Spectra* 1998; **14**:469–500.
14. Cordova P, Deierlein G, Mehanny S, Cornell C. Development of a two parameter seismic intensity measure for probabilistic assessment procedure. *Second U.S.-Japan Workshop on Performance-Based Earthquake Engineering Methodology for Reinforced Concrete Building Structures*, Sapporo, Japan, PEER Center, University of California, Berkeley, 2000; 195–214.
15. Kurama Y, Farrow K. Ground motion scaling methods for different site conditions and structure characteristics. *Earthquake Engineering & Structural Dynamics* 2003; **32**(15):2425–2450.
16. Alavi B, Krawinkler H. Behavior of moment-resisting frame structures subjected to near-fault ground motions. *Earthquake Engineering and Structural Dynamics* 2004; **33**(6):687–706.
17. Bazzurro P, Luco N. Parameterization of non-stationary acceleration time histories. Lifelines Program Project 1 G00 Addenda. Pacific Earthquake Engineering Research (PEER) Center, University of California: Berkeley, CA, 2004; 83 pp.
18. Kalkan E, Chopra AK. Practical guidelines to select and scale earthquake records for nonlinear response history analysis of structures. U.S. Geological Survey Open-File Report 2010–1068, 2010; 126.
19. Kalkan E, Chopra AK. Modal-pushover-based ground motion scaling procedure. *Journal of Structural Engineering* 2011; **137**(3):289–310.
20. Kalkan E, Kwong NS. Documentation for assessment of modal pushover-based scaling procedure for nonlinear response history analysis of “ordinary standard” bridges. U.S. Geological Survey Open-File Report 2010–1328, 2011; 58.
21. Haselton C. Evaluation of ground motion selection and modification methods: predicting median interstory drift response of buildings. Pacific Earthquake Engineering Research (PEER) Center, California State University: Chico, CA, 2009; 201–219.
22. Dyke S, Spencer B, Sain M. An experimental study of MR dampers for seismic protection. *Smart Materials & Structures* 1998; **7**(5):693–703.
23. Mo Y, Lee Y. Shake table tests on small-scale low-rise structural walls with various sections. *Magazine of Concrete Research* 2000; **52**(3):177–184.
24. Rodriguez M, Restrepo J, Blandon J. Shaking table tests of a four-story miniature steel building – model validation. *Earthquake Spectra* 2006; **22**(3):755–780.
25. Lafortune P, McCormick J, DesRoches R. Testing of superelastic recentering pre-strained braces for seismic resistant design. *Journal of Earthquake Engineering* 2007; **11**(3):383–399.
26. ICBO. International building code. *International Conference of Building Officials*, Whittier, CA, 2009.
27. ICBO. California building code. *International Conference of Building Officials*, Whittier, CA, 2010.
28. ASCE. Minimum design loads for buildings and other structures. American Society of Civil Engineers, ASCE Standard No. ASCE/SEI 7–05, Reston, VA, 2006.
29. ASCE. Minimum design loads for buildings and other structures. American Society of Civil Engineers, ASCE Standard No. ASCE/SEI 7–10, Reston, VA, 2010.
30. Reyes JC, Kalkan E. Required number of records for ASCE/SEI 7 ground motion scaling procedure. U.S. Geological Survey Open-File Report 2011–1083, 2011; 34.

31. Anderson J, Bertero VV. Uncertainties in establishing design earthquakes. *Journal of Structural Engineering* 1987; **113**(8):1709–1724.
32. Naeim F, Anderson J. Classification and evaluation of earthquake records for design. CE 93–08, Dept. of Civil Engineering, Univ. of Southern California, Los Angeles, CA, 1993.
33. Naeim F, Anderson J, Jain S. A data base of earthquake records for design. *Fifth U.S. National Conference on Earthquake Engineering*, Oakland, CA, 1994; 263–272.
34. Baker JW. Quantitative classification of near-fault ground motions using wavelet analysis. *Bulletin of the Seismological Society of America* 2007; **97**(5):1486–1501.
35. Kalkan E, Kunnath SK. Effects of fling-step and forward directivity on the seismic response of buildings. *Earthquake Spectra* 2006; **22**(2):367–390.
36. Kalkan E, Kunnath SK. Relevance of absolute and relative energy content in seismic evaluation of structures. *Advances in Structural Engineering* 2008; **11**(1):17–34.
37. PEER next generation of attenuation (NGA) project ground motions database. Pacific Earthq. Eng. Res. Center, [http://peer.berkeley.edu/products/strong\\_ground\\_motion\\_db.html](http://peer.berkeley.edu/products/strong_ground_motion_db.html).
38. Neter J, Kutner MH, Nachtsheim CJ, Wasserman W. *Applied Linear Statistical Models* (4th edn). McGraw-Hill: Boston, MA, 1996; 1408 p.
39. Goel RK, Chopra AK. Period formulas for moment-resisting frame buildings. *Journal of Structural Engineering* 1997; **123**(11):1454–1461.
40. Craig RR, Kurdila AJ. *Fundamentals of Structural Dynamics* (2nd edn). John Wiley and Sons, Inc.: Hoboken, NJ, 2006; 74–75
41. Mazzoni S, McKenna F, Scott M, Fenves G. Open system for earthquake engineering simulation: OpenSees command language manual. University of California, Berkeley, CA. (available online at <http://opensees.berkeley.edu/>)